arXiv:astro-ph/9812076v1 3 Dec 1998

Physical Structure of Small Wolf-Rayet Ring Nebulae

You-Hua Chu[1], Kerstin Weis[1,2]
Astronomy Department, University of Illinois, 1002 W. Green Street, Urbana, IL 61801
Electronic mail: chu@astro.uiuc.edu, kweis@platon.ita.uni-heidelberg.de

Donald R. Garnett[1,3]
Astronomy Department, University of Minnesota, 116 Church Street, S. E., Minneapolis, MN 55455
Electronic mail: dgarnett@as.arizona.edu

ABSTRACT

We have selected the seven most well-defined WR ring nebulae in the LMC (Br 2, Br 10, Br 13, Br 40a, Br 48, Br 52, and Br 100) to study their physical nature and evolutionary stages. New CCD imaging and echelle observations have been obtained for five of these nebulae; previous photographic imaging and echelle observations are available for the remaining two nebulae. Using the nebular dynamics and abundances, we find that the Br 13 nebula is a circumstellar bubble, and that the Br 2 nebula may represent a circumstellar bubble merging with a fossil main-sequence interstellar bubble. The nebulae around Br 10, Br 52, and Br 100 all show influence of the ambient interstellar medium. Their regular expansion patterns suggest that they still contain significant amounts of circumstellar material. Their nebular abundances would be extremely interesting, as their central stars are WC5 and WN3-4 stars whose nebular abundances have not been derived previously. Intriguing and tantalizing implications are obtained from comparisons of the LMC WR ring nebulae with ring nebulae around Galactic WR stars, Galactic LBVs, LMC LBVs, and LMC BSGs; however, these implications may be limited by small-number statistics. A SNR candidate close to Br 2 is diagnosed by its large expansion velocity and nonthermal radio emission. There is no indication that Br 2's ring nebula interacts dynamically with this SNR candidate.

Subject headings: stars: Wolf-Rayet - stars: mass-loss - ISM: bubbles - ISM: kinematics and dynamics - Magellanic Clouds

---

[1]Visiting astronomer, Cerro Tololo Inter-American Observatory, National Optical Astronomy Observatories, operated by the Association of Universities for Research in Astronomy, Inc., under a cooperative agreement with the National Science Foundation.

[2]Current address: Institut für Theoretische Astrophysik, Tiergartenstr. 15, D-69121 Heidelberg, Germany.

[3]Current address: Steward Observatory, University of Arizona, Tucson, AZ 85721.

1. Introduction

Wolf-Rayet (WR) stars are characterized by broad emission lines that are indicative of fast stellar winds and high mass loss rates. The fast stellar wind sweeps up the ambient medium into a dense expanding shell, called a wind-blown bubble. Wind-blown bubbles in a homogeneous medium have been modeled by, for example, Castor, McCray, & Weaver (1975), Steigman, Strittmatter, & Williams (1975), and Weaver et al. (1977). However, these models cannot be readily applied to bubbles blown by WR stars because WR stars are evolved massive stars and their progenitors' mass loss has drastically modified their gaseous surroundings. The physical conditions of a WR star's ambient medium are highly dependent on the star's evolutionary history and mass loss history.

WR stars are divided into WN (nitrogen) and WC (carbon-oxygen) sequences; the WN sequence is further divided into excitation classes WN2–9 and the WC sequence into WC4–9 (van der Hucht et al. 1981). These diverse types of WR stars have different initial masses and evolutionary paths (Langer et al. 1994). It is conceivable that ring nebulae around WR stars must have a variety of origins and physical conditions.

The formation of WR bubbles has been calculated both analytically (García-Segura & Mac Low 1995a) and numerically (García-Segura & Mac Low 1995b). Hydrodynamic models of bubbles have been produced for WR stars descendent from luminous blue variables (LBVs; García-Segura, Mac Low, & Langer 1996, hereafter GML96) and from red supergiants (RSGs; García-Segura, Langer, & Mac Low 1996, hereafter GLM96), respectively. These models conclude that the abundances, morphology, and kinematics of a WR bubble can be used to diagnose the evolutionary status of the bubble and to determine whether the central WR star is a descendant of a LBV (e.g., RCW 58) or a RSG (e.g., NGC 6888).

It is of interest to compare these models to a large number of WR bubbles to determine the nature of the bubbles and the applicability of the models. Recent CCD surveys have found many new WR ring nebulae in our Galaxy (Miller & Chu 1993; Marston et al. 1994a, 1994b) and in the Large Magellanic Cloud (LMC; Dopita et al. 1994). These ring nebulae provide excellent samples of WR bubbles for comparisons with models.

We have begun to study the LMC sample because the extinction is small, the distance is well-known, and the LMC WR bubbles can be easily studied with long-slit spectrographs. Table 1 lists the most well-defined small WR ring nebulae in the LMC. The WR stars Br 2, Br 10, Br 13, Br 48, Br 52, and Br 100 were from Breysacher (1981), and the star Br 40a was from Conti & Garmany (1983). We have obtained high-dispersion echelle/CCD observations for five of these small WR rings to determine their dynamic structures and to diagnose their nature. In this paper we report the observations (§2), interpret the data (§3), and compare the LMC WR ring nebulae to the hydrodynamic models of GML96 and GLM96, and compare them to the ring nebulae around Galactic WR stars, LBVs, and blue

supergiants (§4). A summary is given at the end (§5).

2. Observations

2.1. Imaging

We have obtained emission-line images of five small WR ring nebulae in the LMC using CCD cameras on the 0.9 m telescope at Cerro Tololo Inter-American Observatory (CTIO). In December 1991, the nebulae around Br 2 and Br 13 (Breysacher 1981) were imaged in the Hα and [O III] λ5007 lines with a Tektronix 1024×1024 CCD (Tek1024#1). The pixel size was 0.″4 pixel^{-1} and the field of view was 6.′8×6.′8. In January 1996, the nebulae around Br 40a, Br 48, and Br 52 were imaged in the [O III] λ5007 line with a Tektronix 2048×2048 CCD (Tek2K3). The pixel size was 0.″4 pixel^{-1} and the field of view was 13.′5×13.′5.

The exposure time for each image was typically 900 s. The ring nebula around Br 13 is so faint that two 900 s exposures were averaged together to produce the final image in each filter. Images of the five LMC WR ring nebulae are presented in Figure 1. Note that the Hα images include contributions of the [N II] $\lambda\lambda$6548, 6583 lines, as the Hα filter was centered at 6575 Å with a FWHM of 14 Å. Using the line intensities measured by Garnett & Chu (1994), we find that the [N II] contribution to the Hα images is <1.5% for the Br 2 nebula and <7% for the Br 13 nebula.

2.2. Echelle Spectroscopy

High-dispersion spectroscopic observations of five LMC WR rings were obtained with the echelle spectrograph on the 4 m telescope at CTIO in January 1996. The spectrograph was used in a long-slit mode by inserting a post-slit Hα filter (6563/75 Å) and replacing the cross-disperser with a flat mirror. A 79 lines mm^{-1} echelle grating and the long focus red camera were used. The detector was a Tektronix 2048×2048 CCD (Tek2K4). The pixel size was 0.08 Å pixel^{-1} along the dispersion and 0.″26 pixel^{-1} in the spatial axis. The slit length was effectively limited by vignetting to $\sim 4'$. Both Hα λ6563 and [N II] $\lambda\lambda$6548, 6583 lines were covered in this setup. The slit-width was 250 μm, or 1.″64, leading to an instrumental FWHM of ∼14 km s^{-1} at the Hα line. Thorium-Argon lamp exposures were obtained for wavelength calibration and geometric distortion correction.

The journal of echelle observations is given in Table 2, and the echellograms of the Hα and the [N II] λ6583 lines are shown in Figure 2. Each panel covers 38.48 Å along the dispersion (the horizontal axis), and 2′ for Br 2 and Br 13 and 4′ for Br 40a, Br 48, and Br 52 along the slit (the vertical axis). The narrow, unresolved lines are telluric Hα and OH lines (Osterbrock et al. 1996), which provide convenient references for fine-tuning the

wavelength calibration. The OH 6-1 P2(3.5)6568.779 line is unfortunately blended with the LMC Hα line. This OH line, corresponding to the Hα line at a heliocentric velocity of $V_{hel} \sim 275$ km s^{-1}, can be seen on the left side of the Hα line of the Br 52 nebula (Figure 2).

3. Physical Structure of the Five WR Rings

3.1. Br 2

The ring nebula around Br 2 was at first identified to be the 3′ shell nebula to the south of Br 2 (Rosado 1986). It was later discovered in higher resolution images that a 28″ × 18″ arc surrounds Br 2 (Dopita et al. 1994). This small arc has a morphology similar to that of NGC 6888, but has a much higher excitation and emits He II λ4686 line (Pakull 1991). The contrast between this arc and the background H II region is higher in Hα images than in [O III] images (see Figure 1).

We assume that the small arc is the bona fide ring nebula of Br 2. The echelle observations along position angles PA = 120° and 135° (near the minor axis) show a broader Hα line within the arc; the FWHM of the Hα line is 42±1 km s^{-1} near Br 2, and 32±1 km s^{-1} outside the arc. The centroid of the Hα line near Br 2 is blue-shifted by 3 km s^{-1} with respect to the background H II region velocity at V_{hel} = 253±2 km s^{-1}. This small velocity shift prohibits an unambiguous decomposition of the broadened line into multiple components. Fortunately, the He II λ6560.18[4] line is detected within and beyond the arc. The He II line is less confused by the background H II region emission, hence provides better kinematic diagnostics for Br 2's ring.

The He II line is curved. In the background H II region exterior to the arc, the centroid velocity of the He II line, 250±3 km s^{-1}, is similar to that of the Hα line. Near Br 2 the He II line is blue-shifted by 16±2 km s^{-1} with respect to the He II velocity exterior to the arc. A similar He II velocity structure is seen in the echellogram taken along PA = 45° near the major axis the arc. This velocity structure indicates that the stellar wind of Br 2 has accelerated the ambient medium by 16 km s^{-1}. The accelerated ambient medium is probably interstellar matter, as it has normal LMC interstellar abundances (Garnett & Chu 1994).

It is worth noting that a supernova remnant (SNR) candidate is detected to the northwest of Br 2's ring along PA = 120° and 135°. This SNR candidate appears as a

[4]We have calibrated the wavelength of the He II line using echelle observations of the H II region N44C, of which the Hα and He II lines are narrow. We find the He II line to be at 2.60±0.05 Å shorter wavelength than the Hα line. For an Hα wavelength of 6562.78 Å, the He II line will be at 6560.18 Å.

high-velocity feature, with velocity offsets up to 150 km s^{-1}, extending from the Br 2's ring to the northwest for at least 80″. Our long-slit low-dispersion spectra of this region also show enhanced [S II] and [O I] lines characteristic of SNRs (Garnett & Chu 1994).

3.2. Br 13

The ring nebula of Br 13 is elongated along the position angle 33°. Its semi-major axis is 20″ long and its semi-minor axis 16″, corresponding to 5 pc and 4 pc, respectively. Only the northwestern half of the ring is detected in our Hα and [O III] images.

Our echelle observation along the E–W direction shows a stationary component from the background H II region and a velocity-position ellipse from the ring nebula. The velocity-position ellipse, indicating an expanding shell, is detected in both the Hα and [N II]λ6583 lines, although the latter has a much lower S/N ratio. As in the direct images, the surface brightness of the expanding shell is not uniform. The receding side of the shell is detected for 19″ on the west side of Br 13 and ∼20″ on the east, but the approaching side is detected only on the west side. The largest velocity split, 160 km s^{-1}, is detected near the shell center.

To determine the expansion velocity, we need to know the systemic velocity of the nebula. Br 13 and its ring nebula are projected against the outskirts of the H II region DEM L 56 (Davies, Elliott, & Meaburn 1976) which has a heliocentric velocity of 304 km s^{-1}. However, this velocity does not necessarily represent the velocity of Br 13's ring nebula because the ring nebula consists of ejected stellar material (Garnett & Chu 1994) and Br 13 may not have the same origin and systemic velocity as DEM L 56. The stellar He II λ6560 line profile of Br 13, having a FWHM of ∼1080 km s^{-1} and containing an unknown amount of stellar Hα emission, cannot be used to determine the radial velocity of Br 13. We have to resort to the nebular velocities to assess the systemic velocity of Br 13 and its ring nebula.

The echelle data show that the western tip of the ring nebula's velocity-position ellipse converges to the H II region velocity, but the eastern tip is not detected. The faint velocity-position ellipse in the [N II] line appears to be slightly tilted, with the western end toward lower velocity and the eastern end higher velocity. Since the [N II] line is detected at a very low S/N, it is difficult to determine the exact amount of line tilt. If the expansion is symmetric with respect to the central star, the radial velocities of the approaching and receding sides of the shell at the center, 237 and 397 km s^{-1}, would imply a systemic velocity of 317 km s^{-1} and an expansion velocity of 80 km s^{-1} along the line of sight toward Br 13. Br 13's ring nebula would be moving at +13 km s^{-1} relative to the background H II region. This relative motion may be responsible for the higher surface brightness of the leading side of the shell. Nevertheless, we cannot confidently rule out the possibility that Br

13 and its ring nebula do have the same systemic velocity as the H II region DEM L 56, and the expansion of Br 13's circumstellar bubble is asymmetric, with the expansion velocity being 67 km s^{-1} on the approaching side and 93 km s^{-1} on the receding side.

3.3. Br 40a

Br 40a is located in the northwestern quadrant of the H II complex N206 (Henize 1956), or DEM L 221. Hα images show a parabolic-shaped arc around Br 40a, which has been suggested to be a ring nebula (Dopita et al. 1994). However, our [O III] image shows that the Hα arc is composed of two filaments with different excitations. The eastern part of the Hα arc has such a low excitation that it is not detected in our [O III] image. The shape of the Hα arc is probably fortuitous.

Our echelle observation has a N–S oriented slit passing through Br 40a. Within the nebula around Br 40a, no line split is detected, but the centroid of the Hα line is red-shifted by several km s^{-1} with respect to that of the background H II region. The Hα velocity varies from 232 km s^{-1} southward of Br 40a's ring to 242–245 km s^{-1} within the boundary of Br 40a's ring, and to 237 km s^{-1} at large distances to the north. A He II-emission region around Br 40a has been reported by Niemela (1998); however, our echelle observation did not detect the He IIλ6560 line.

The velocity pattern of Br 40a's ring nebula does not suggest an expanding shell, but does suggest interactions between Br 40a and its surrounding medium. The anomalous velocity in the small nebula round Br 40a is probably caused by the fast stellar wind accelerating the dense interstellar medium on the far side of the star.

3.4. Br 48

The ring nebula around Br 48 is inside the H II region DEM L 231. The ring has a "double rim" morphology that resembles a tilted short cylinder. This distinct morphology is remarkably reminiscent of the Ring Nebula, although their nature and dynamic structures are completely different. Br 48's ring has a dimension of $95'' \times 70''$, or 24×17 pc, and the surrounding H II region is about 50 pc in diameter.

The velocity field of DEM L 231 has been previously studied with the same echelle spectrograph on the same telescope but using photographic plates (Chu 1983). Based on those photographic data, it was deduced that Br 48 interacts with a tilted slab of interstellar gas and that no three-dimension expanding shell is present. This basic picture is still supported by our new observations using a more sensitive detector.

Our new echelle observation samples a E–W cut through the central star. An apparent

velocity gradient is detected in the H II region, with the heliocentric velocity varying from 311 km s^{-1} on the east to 297 km s^{-1} on the west. Within the central cavity, the Hα line is centered at 295–300 km s^{-1}. Relative to this central velocity, the inner rim of Br 48's ring is blue-shifted at $V_{hel} \sim 294$ km s^{-1} on the east side, and red-shifted at $V_{hel} \sim 306$ km s^{-1} on the west side. This indicates that Br 48 indeed interacts with a slab of gas and that this slab is tilted with the east side toward us.

No high-velocity components are detected near the central cavity. The apparent velocity FWHM at the central cavity reaches 45 km s^{-1}, as opposed to 30±1 km s^{-1} in the brighter and more quiescent parts of the ring or the H II region. Quadratically subtracting a thermal FWHM of 21 km s^{-1} (for 10^4 K) and an instrumental FWHM of 14 km s^{-1}, we derive a turbulent FWHM of 37 km s^{-1} for the central cavity and 16 km s^{-1} in the bright (quiescent) region. If the broadening of velocity profiles at the central cavity is caused by an expansion, the expansion velocity cannot be larger than 18±1 km s^{-1}.

3.5. Br 52

The ring nebula of Br 52 was once thought to be the 40″ triangular-shaped nebula to the east of the star (Chu & Lasker 1980). Recent CCD images have detected the fainter part of the ring nebula to the southwest of Br 52 (Dopita et al. 1994). The [O III] image in Figure 1 shows a complete shell structure, although the southwestern half is fainter.

Our new echelle observation has a E–W oriented slit centered on Br 52. The Hα line is dominated by one bright component. The heliocentric velocity of this main component is 320 km s^{-1} outside the ring nebula. Within the ring nebula, the velocity of the main Hα component is marginally blue-shifted, by 2 km s^{-1}, on the west side of Br 52 and red-shifted by up to 5 km s^{-1} on the east side of Br 52. An additional faint, red-shifted Hα component is present within the ring nebula on the west side of Br 52. The heliocentric velocity of this component reaches 370 km s^{-1}, which is offset from the main component by +50 km s^{-1}.

The velocity structure of Br 52's ring nebula indicates a "blister" structure. This ring nebula is most likely an interstellar bubble blown by Br 52 in a medium with a steep density gradient. The bubble/blister expands into the lower-density medium with an V_{exp} of ∼50 km s^{-1}.

4. Discussion

The formation of a WR ring nebula can be qualitatively described by the following scenario (GML96; GLM96). A massive star evolves off the main sequence, passes through a RSG phase or a LBV phase, then lands on a WR phase. During the main sequence stage,

the fast stellar wind sweeps up the ambient interstellar medium to form an interstellar bubble. The copious mass loss during the RSG or LBV phase would form a circumstellar envelope within the central cavity of the main sequence bubble. As the central star evolves into a WR star, the fast WR wind compresses the circumstellar envelope of previous RSG or LBV wind to a dense shell, forming a circumstellar bubble. As the circumstellar bubble expands past the outer edge of the circumstellar envelope, instabilities set in and the dense shell fragments. The circumstellar bubble may collide and merge with the main sequence interstellar bubble or evaporate in the hot shocked WR wind in the interior of the main sequence bubble.

An observed WR ring nebula could be in any of these aforementioned stages. It is conceivable that interstellar bubbles have large dynamic ages and normal (interstellar) abundances, while the circumstellar bubbles have small dynamic ages and anomalous abundances. As a circumstellar bubble merges with the surrounding interstellar bubble, the observed abundances will asymptotically approach the normal (interstellar) abundances. The most telltale physical properties that may distinguish these stages are thus nebular dynamics and abundances. However, it must be born in mind that large variations exist in the history of stellar mass loss and the distribution of ambient interstellar medium; therefore, even detailed information on dynamics and abundances may not lead to a unique interpretation.

We are extending the study of WR ring nebulae to the LMC sample and have selected the seven most well-defined WR rings in the LMC from the survey by Dopita et al. (1994). These seven ring nebulae, listed in Table 1, not only have distinct ring or arc morphology but also have sizes in the range of 5 to 40 pc, so that these ring nebulae may be the true counterparts of the archetypical WR rings, such as NGC 2359, NGC 6888, and S 308 in the Galaxy (Johnson & Hogg 1965).

We will first discuss the nature of these seven LMC WR ring nebulae and compare them to the Galactic WR ring nebulae. We will further compare the WR ring nebulae to ring nebulae around LBVs and blue supergiants (BSGs). As these different spectral types represent different evolutionary stages of massive stars, the comparison of physical properties among their ring nebulae may help us understand the evolutionary aspects of these stars. The size, expansion velocity, "dynamic timescale", and N/O abundance ratios of these nebulae are tabulated in Table 3. The "dynamic timescale" is defined as the expansion velocity divided by the radius. This dynamic timescale scales with the dynamic age of the nebula, but is not equal to the dynamic age which depends on whether the expansion has been accelerated or decelerated since the initial formation.

4.1. LMC and Galactic WR Ring Nebulae

The kinematic structure of each of the seven selected LMC WR ring nebulae (Chu 1983; this paper) suggests interactions between the fast stellar wind and the ambient medium. In some nebulae, especially those around Br 40a and Br 48, the kinematic structure is so irregular that it cannot be approximated as an expanding shell. These irregular motions are clearly caused by the large density variations in the ambient interstellar medium; consequently, the kinematic structure of these nebulae cannot be used to derive unambiguous information on the stellar mass loss history. For the rest of this discussion we will concentrate on only the other five nebulae that have well-behaved expansion properties.

For comparison, we have selected six Galactic WR ring nebulae, listed in Table 3, based on their well-observed dynamics and abundances. Relative to a Galactic interstellar N/O ratio of $\sim$0.07$\pm$0.01 (Shaver et al. 1983), S308, RCW 58, M 1-67, and NGC 6888 are obviously enriched and must contain stellar ejecta. NGC 2359 and NGC 3199, on the other hand, show little abundance anomaly, indicating that these nebulae are dominated by interstellar material. These two nebulae also have the most irregular expansion patterns and the smallest expansion velocities. These dynamic properties and N/O abundance ratios suggest that the circumstellar bubbles of NGC 2359 and NGC 3199 have merged with the fossil main sequence interstellar bubbles. Using the detailed fragmentation morphology, GLM96 and GML96 conclude that NGC 6888's WR star has evolved through a RSG phase, and RCW 58's WR star has evolved through a LBV phase.

The LMC WR ring nebulae do not have as many observations of abundances available as the Galactic nebulae. Only two LMC nebulae, around Br 2 and Br 13, have been observed (Garnett & Chu 1994). Compared to the LMC interstellar value of N/O $\sim$0.04 (Garnett 1998), the Br 13 nebula has clearly anomalous abundances while the Br 2 nebula is marginally anomalous. The Br 13 nebula must be a circumstellar bubble; its regular expansion pattern and small dynamic timescale both support this explanation. The spectral type of Br 13, WN8, is the same as that of WR40, the central star of RCW 58; the N/O ratio of the Br 13 nebula is similar to that of RCW 58. If the progenitor of WR40 was a LBV, it is then possible that the progenitor of Br 13 was also a LBV. A high-resolution image of the Br 13 nebula would be useful in determining whether the fragmentation of the nebula is consistent with those expected for a LBV progenitor (GML96). The N/O ratio of the Br 2 nebula indicates that it might be a circumstellar bubble merging with a main sequence interstellar bubble. This explanation is supported by the large dynamic timescale and small expansion velocity of the Br 2 nebula.

The other three LMC WR ring nebulae, around Br 10, Br 52, and Br 100, do not have abundance observations. Their large sizes and surface brightness variations indicate that they must be interacting with the ambient interstellar medium. However, these three nebulae have relatively large expansion velocities and quite regular expansion pattern,

especially the Br 10 nebula. If the LMC WR nebulae behave similarly to the Galactic WR nebulae, we may expect that these three nebulae are not yet dominated by interstellar material. The spectral types of these three central stars are WC5 and WN3-4. No abundances have been derived for circumstellar nebulae of WC5 or WN3-4 stars in either the Galaxy or the Magellanic Clouds. New abundance observations of these three WR nebulae would be most interesting, as they could place constraints on the evolution of progenitors for these spectral types.

4.2. Comparison with Ring Nebulae around Other Massive Stars

We have included in Table 3 a number of Galactic and LMC LBV nebulae whose nebular dynamics have been well observed. The Galactic LBV nebulae are all smaller and younger than the Galactic WR ring nebulae. Among the Galactic LBV nebulae, the smallest one has the smallest dynamic timescale and the lowest expansion velocity. If these four Galactic LBVs evolve similarly, their nebulae must have gone through a rapid acceleration during the LBV phase.

The LMC LBV nebulae appear to be generally larger than the Galactic LBV nebulae. This could be completely caused by a combination of small-number statistics and difficulty in resolving and detecting small LBV nebulae in the LMC where 1 pc subtends only 4″. It is noteworthy, however, that the LMC LBV nebulae have smaller expansion velocities than the Galactic counterparts. This relation, if it holds for a larger number of LMC LBV nebulae, may indicate a difference in the mass loss properties between the LMC LBVs and the Galactic LBVs.

It is interesting to compare the Br 13 nebula to the LMC LBV nebulae. The dynamic timescale of the Br 13 nebula is comparable to those of the LMC LBV nebulae of R127 and S119, although the Br 13 nebula is much larger and expands much faster. This comparison suggests that the progenitor of Br 13 could not have been a LBV similar to R127 or S119.

Finally, we examine two ring nebulae around LMC blue supergiants (BSGs). The ring nebula around the O9f star Sk−69 279 is recently discovered by Weis et al. (1997b). Its high [N II]λ6583/Hα ratio, $\sim$0.7, is consistent with that expected in a N-enriched ejecta nebula. Its expansion velocity, only 14 km s^{-1}, is lower than those of all WR and LBV nebulae listed in Table 3. Its size is larger than that of every known LBV nebula, but comparable to those of small WR ring nebulae. The exact abundances of Sk−69 279's nebula are unknown, hence it is uncertain whether the nebula has swept up a significant amount of interstellar material and its expansion has subsequently been slowed down. Future abundance observations are needed to determine the evolutionary status of Sk−69 279 with respect to RSG, LBV, and WR phases. The ring nebula around the B3I star Sk−69 202, better known as the progenitor of SN 1987A, is small compared to ring nebulae around

other massive stars. Its expansion velocity is the smallest. Clearly, the size and dynamics of Sk−69 202's ring nebula suggest that Sk−69 202 could not have gone through a WR phase. This is consistent with the relatively low mass (20 $M_\odot$) inferred for the supernova SN 1987A's progenitor.

4.3. A SNR Candidate Near Br 2

The echelle observations of Br 2 reveal a high-velocity feature to the northwest of Br 2. The echellogram of the slit position centered on Br 2 along the position angle 120° shows high-velocity material projected from the vicinity of Br 2 to almost 90″ northwest of Br 2. The slit position centered at 10″N, 35″W of Br 2 along the N-S direction shows high-velocity material over 110″, or 28 pc, along the slit (Figure 2). The velocity structure and size are very similar to those of known SNRs in the Magellanic Clouds, particularly the SNR N19 (0045−73.4) in the Small Magellanic Cloud (Chu & Kennicutt 1988). The radio continuum emission of this region is brighter than those of H II regions of comparable or even higher Hα surface brightnesses (Haynes et al. 1991), indicating a nonthermal radio emission. Thus, this high-velocity feature most likely originates from a SNR at an age of a few $\times 10^4$ yr.

Br 2's ring nebula is unusual in two respects. First, He II emission is detected in the ring nebula. Second, Br 2's ring overlaps the projected position of a SNR candidate. However, the He II emission cannot be caused by a dynamic interaction between the ring nebula and the SNR, as the He IIλ6560 line does not show violent velocities and the Hα line of the ring nebula does not show continuous high-velocity wings. The SNR is probably just projected by chance to the vicinity of Br 2 and its ring nebula.

5. Summary

We have selected the seven most well-defined WR ring nebulae in the LMC to study their physical nature and evolutionary stages. New images and echelle observations have been obtained for five of these nebulae; previous observations (Chu 1983) are available for the two remaining nebulae. Only five of these nebulae (Br 2, Br 10, Br 13, Br 52, and Br 100) have well-behaved expansion pattern to warrant further discussion. Of these five nebulae, Br 2's and Br 13's ring nebulae have abundance information available (Garnett & Chu 1994).

Based on nebular dynamics and abundances, we suggest that the Br 13 nebula is a circumstellar bubble, and that the Br 2 nebula may represent a circumstellar bubble merging with a fossil main-sequence interstellar bubble. The nebulae around Br 10, Br 52, and Br 100 all show influence of the ambient interstellar medium. Their regular expansion

patterns suggest that they still contain significant amounts of circumstellar material. The abundances of these nebulae would be extremely interesting, as their central stars are WC5 and WN3-4 stars whose nebular abundances have never been derived before.

The LMC WR ring nebulae do not differ significantly from their Galactic counterparts. Comparisons between WR ring nebulae and ring nebulae around other massive stars, such as LBVs and BSGs, yield intriguing and tantalizing implications on stellar evolution and mass loss history. However, the credibility of these implications is limited by a small number statistics. Future observations of a larger number of nebulae are needed to confirm these results.

YHC acknowledges the support of NASA LTSA grant NAG 5-3246. DRG acknowledges support from NASA LTSA grant NAG 5-6416.

Table 1: Small Wolf-Rayet Ring Nebulae in the Large Magellanic Cloud

WR[a] Star	Nebula[b] Name	Size (arcsec)
Br 2	in DEM L 6	28×18
Br 10	in DEM L 39	190×100
Br 13	in DEM L 56	41×22
Br 40a[c]	in DEM L 221	75×40
Br 48	DEM L 231	95×70
Br 52	DEM L 240	100×70
Br 100	DEM L 315	125×90

Notes:

[a] Breysacher 1981.

[b] Davies, Elliott, & Meaburn 1976.

[c] Conti & Garmany 1983.

Table 2: Journal of Echelle Observations

WR Star	Slit Number	Offset from Star	Position Angle	Exposure (sec)	Date of Observation
Br 2	1	–	120°	2×900	96/1/9
Br 2	2	5″W	135°	900	96/1/10
Br 2	3	4″N, 4″W	45°	900	96/1/11
Br 2	4	10″N, 35″W	0°	900	96/1/10
Br 13	1	–	90°	900	96/1/10
Br 40a	1	–	0°	900	96/1/11
Br 48	1	–	90°	900	96/1/10
Br 52	1	–	90°	600	96/1/10

Table 3: Ring Nebulae around Massive Stars

Star Name	Spectral Type	Nebula Name	Size (pc)	V_{exp} (km s^{-1})	V_{exp}/R (yr)	N/O	References.
Br 2	WN4	in DEM L 6	7×4.5	16	1.8×10^5	0.070±0.015	1,2
Br 10	WC5	in DEM L 39	47×25	42	4.3×10^5	–	3
Br 13	WN8	in DEM L 56	10×5.5	80	6.3×10^4	0.57±0.18	1, 2
Br 52	WN4+OB	DEM L 240	25×17.5	50	2.1×10^5	–	1, 3
Br 100	WN3-4	DEM L 315	31×22.5	47	2.8×10^5	–	3
WR 5	WN5	S 308	14.4	60	1.2×10^5	1.66	4, 5
WR 7	WN4	NGC 2359	6.5	20	1.6×10^5	0.112	5, 6
WR 18	WN5	NGC 3199	19×15	20	4.3×10^5	0.148	5, 7
WR 40	WN8	RCW 58	8×6	110	3.2×10^4	0.501	5, 6
WR 124	WN8	M 1-67	2	42	2.4×10^4	2.95	5, 8
WR 136	WN6	NGC 6888	4.2×6.3	80	3.3×10^4	1.86	5, 6
AG Car	LBV	AG Car nebula	1.1×1.0	70	7.1×10^3	5.74±2.25	9, 10
He3-519	LBV	He3-519	2.2	62	1.8×10^4	–	11
HD 168625	LBV	HD 168625 nebula	0.06	20	3.0×10^3	–	12
HR Car	LBV	HR Car nebula	1.3×0.7	~ 100	5.0×10^3	>3	13, 14
R127	LBV	R127 nebula	1.9×2.2	28	7.1×10^4	0.89±0.40	15, 16
S119	LBV	S119 nebula	2.1×1.9	25	8.0×10^4	1.41–2.45	16, 17
Sk−69 279	O9f	Sk−69 279 nebula	4.5	14	1.6×10^5	–	18
Sk−69 202	B3I	(SN 1987A's ring)	0.4	10	2.0×10^4	1.6	19, 20

REFERENCES. – (1) This paper; (2) Garnett & Chu 1994; (3) Chu 1983; (4) Chu et al. 1982; (5) Esteban et al. 1992; (6) Chu 1988; (7) Chu 1982; (8) Solf & Carsenty 1982; (9) Smith 1991; (10) Smith et al. 1997; (11) Smith et al. 1994; (12) Hutsemekers et al. 1994; (13) Weis et al. 1997a; (14) Nota et al. 1997; (15) Appenzeller et al. 1987; (16) Smith et al. 1998; (17) Nota et al. 1994; (18) Weis et al. 1997b; (19) Crotts & Heathcote 1991; (20) Panagia et al. 1996.

REFERENCES

Appenzeller, I., Wolf, B., & Stahl, O. 1987, in Instabilities in Luminous Early-Type Stars, ed. H. J. G. L. M. Lamers & C. W. H. de Loore (Dordrecht: Reidel), 241

Breysacher, J. 1981, A&AS, 43, 203

Castor, J., McCray, R., & Weaver, R. 1975, ApJ, 200, L107

Chu, Y.-H. 1982, ApJ, 254, 578

Chu, Y.-H. 1983, ApJ, 269, 202

Chu, Y.-H. 1988, PASP, 100, 986

Chu, Y.-H., Gull, T. R., Treffers, R. R., Kwitter, K. B., & Troland, T. H. 1982, ApJ, 254, 562

Chu, Y.-H., & Kennicutt, R. C. Jr. 1988, AJ, 95, 1111

Chu, Y.-H., & Lasker, B. M. 1980, PASP, 92, 730

Conti, P. S., & Garmany, C. D. 1983, PASP, 95, 411

Crotts, A. P., & Heathcote, S. R. 1991, Nature, 350, 683

Davies, R. D., Elliott, K. H., & Meaburn, J. 1976 MmRAS, 81, 89

Dopita, M. A., Bell, J. F., Chu, Y.-H., & Lozinskaya, T. A. 1994, ApJS, 93, 455

Esteban, C., Vílchez, J. M., Smith, L. J., & Clegg, R. E. S. 1992, A&A, 259, 629

García-Segura, G., & Mac Low, M.-M. 1995a, ApJ, 455, 145

García-Segura, G., & Mac Low, M.-M. 1995b, ApJ, 455, 160

García-Segura, G., Langer, N., & Mac Low, M.-M. 1996, A&A, 316, 133 (GLM96)

García-Segura, G., Mac Low, M.-M., & Langer, N. 1996, A&A, 305, 229 (GML96)

Garnett, D. R. 1998, in IAU Symp. 190, New Views of the Magellanic Cloud, ed. Y.-H. Chu et al., in press

Garnett, D. R., & Chu, Y.-H. 1994, PASP, 106, 626

Haynes, R. F., et al. 1991, A&, 252, 475

Hutsemekers, D., Van Drom, E., Gosset, E., & Melnick, J. 1994, A&A, 290, 906

Johnson, H. M., & Hogg, D. E. 1965, ApJ, 142, 1033

Langer, N., Hamann, W.-R., Lennon, M., Najarro, F., Pauldrach, A. W. A., & Puls, J. 1994, A&A, 290, 819

Marston, A. P., Chu, Y.-H., & García-Segura, G. 1994a, ApJS, 93, 229

Marston, A. P., Yocum, D. R., García-Segura, G., & Chu, Y.-H. 1994b, ApJS, 95, 151

Miller, G., & Chu, Y.-H. 1993, ApJS, 85, 137

Nota, A., Drissen, L., Clampin, M., Leitherer, C., Pasquali, A., Robert, C., Paresce, F., & Robberto, M. 1994, in Circumstellar Media in the Late Stages of Stellar Evolution, ed. R. Clegg et al. (Cambridge: Cambridge Univ. Press), 89

Nota, A., Smith., L. J., Pasquali, A., Clampin, M., & Stroud, M. 1997, ApJ, 486, 338

Osterbrock, D. E., Fulbright, J. P., Martel, A. R., Keane, M. J., Trager, S. C., & Basri, G. 1996, PASP, 108, 277

Pakull, M. W. 1991, in IAU Symp. 143, Wolf-Rayet Stars and Interrelations with Other Massive Stars in Galaxies, ed. K. A. van der Hucht & B. Hidayat (Dordrecht: Kluwer), 391

Panagia, N., Scuderi, S., Gilmozzi, R., Challis, P. M., Garnavich, P. M., & Kirshner, R. P. 1996, ApJ, 459, L17

Rosado, M. 1986, A&A, 160, 211

Shaver, P. A., McGee, R. X., Newton, L. M., Danks, A. C., Pottasch, S. R. 1983, MNRAS, 204, 53

Smith, L. J. 1991, in IAU Symp. 143, Wolf-Rayet Stars and Interrelations with Other Massive Stars in Galaxies, ed. K. A. van der Hucht & B. Hidayat (Dordrecht: Kluwer), 385

Smith, L. J., Crowther, P. A., & Prinja, R. K. 1994, A&A, 281, 833

Smith, L. J., Nota, A., Pasquali, A., Leitherer, C., Clampin, M., & Crowther, P. A. 1998, ApJ, 503, 278

Smith, L. J., Stroud, M. P., Esteban, C., Vílchez, J. M. 1997, MNRAS, 290, 265

Smith, L. J., & Willis, A. J. 1983, A&AS, 54, 229

Solf, J., & Carsenty, U. 1982, A&A, 116, 54

Steigman, G., Strittmatter, P. A., & Williams, R. E. 1975, ApJ, 198, 575

van der Hucht, K. A., Conti, P. S., Lundstrom, I., & Stenholm, B. 1981, Space Sci. Rev., 28, 227

Weaver, R., McCray, R., Castor, J., Shapiro, P., & Moore, R. 1977, ApJ, 218, 377

Weis, K., Duschl, W. J., Bomans, D. J., Chu, Y.-H., & Joner, M. D. 1997a, A&A, 320, 568

Weis, K., Chu, Y.-H., Duschl, W. J., Bomans, D. J. 1997b, A&A, 325, 1157

This preprint was prepared with the AAS LaTeX macros v4.0.

Figure Captions

Fig. 1.— CTIO 0.9-m telescope CCD images of five small WR ring nebulae in the LMC. The images are displayed with the respective WR stars at the field center. North is up and east is to the left. Each panel covers a $2' \times 2'$ or $4' \times 4'$ field of view, as indicated at its lower right corner. The name of the WR star is given at the upper left corner and the filter information upper right corner of the panel.

Fig. 2.— Long-slit echellograms of five small WR ring nebulae in the LMC. The name of the WR star, the slit offset (in units of arcsec) from the central WR star, and the position angle (measured counterclockwisely from the north) of the slit are labeled above each panel. The spatial orientation of the echellogram is marked at the upper right corner of the panel. The wavelength increases to the right. Each panel covers about 38.5 Å, or 1760 km s^{-1} at the Hα line, along the horizontal axis. The nebular Hα and [N II] lines and the telluric ($\oplus$) Hα and OH lines are identified below the bottom panels. The spatial extent of each panel, along the vertical axis, is $2'$ for Br 2 and Br 13, and $4'$ for Br 40a, Br 48, and Br 52. The spatial scales are the same as those for the images in Figure 1.

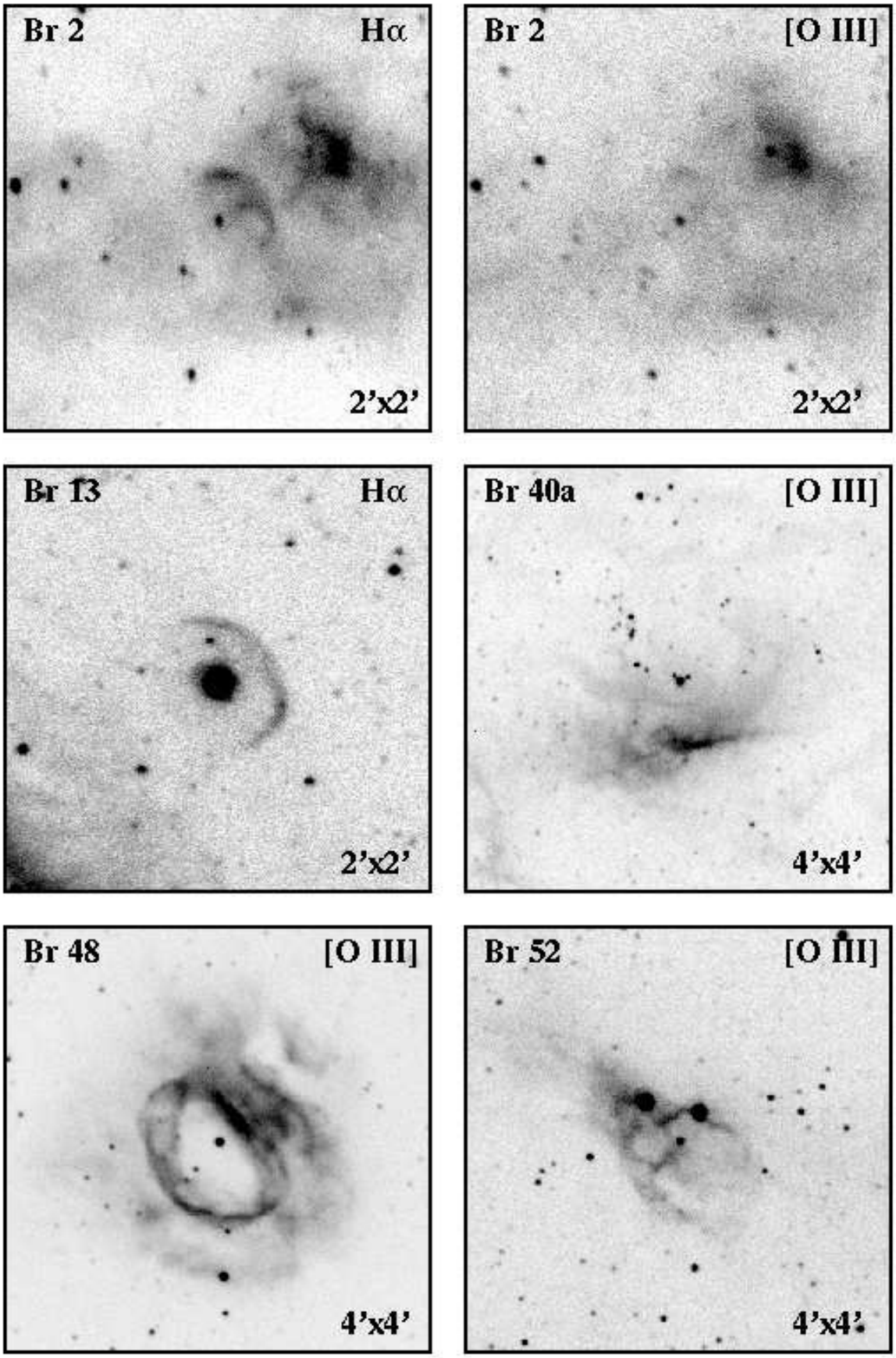
Br 2
Hα
2'x2'
Br 2
[O III]
2'x2'
Br 13
Hα
2'x2'
Br 40a
[O III]
4'x4'
Br 48
[O III]
4'x4'
Br 52
[O III]
4'x4'

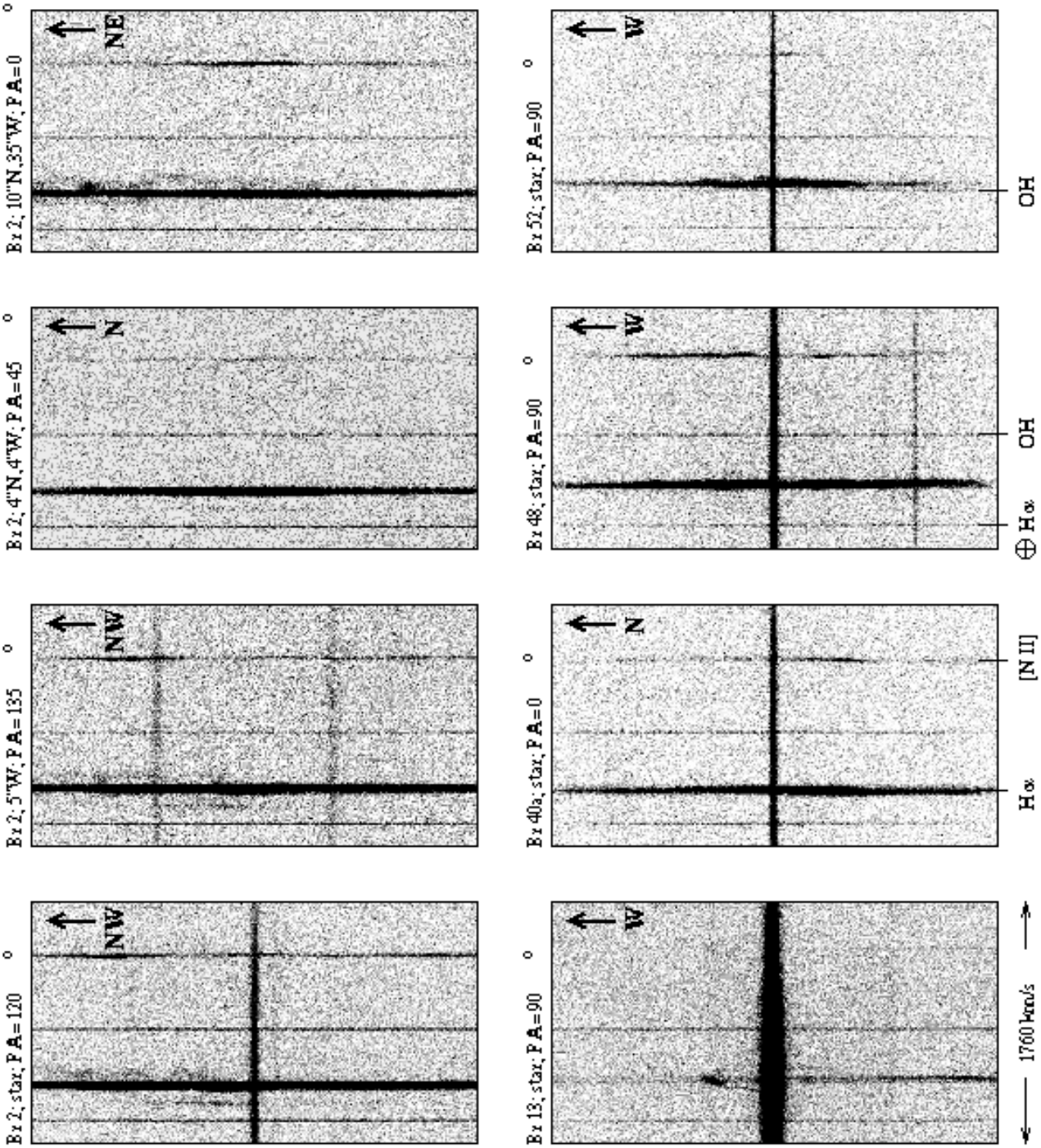
Br 2; star; PA=120°
NW
Br 2; 5"W; PA=135°
NW
Br 2; 4"N,4"W; PA=45°
N
Br 2; 10"N,35"W; PA=0°
NE
Br 13; star; PA=90°
W
Br 40a; star; PA=0°
N
Br 48; star; PA=90°
W
Br 52; star; PA=90°
W
1760 km/s
Hα
[N II]
⊕ Hα
OH
OH